Results from the Longwave Effective Cloud Fraction in the Cloudiness Intercomparison

E.E. Takara and R.G. Ellingson
Department of Meteorology
Florida State University
Tallahassee, Florida

Introduction

While it may seem to be a simple quantity, cloud amount is somewhat elusive. Different types of instruments placed next to each other can give different cloud amounts because they use different parts of the spectrum, have different fields of view, sampling rates, etc. Another consideration is that cloud amount depends on the physical scale under consideration. The cloud amount appropriate for comparison to a single pyrgeometer is not likely to be useful for a grid square with 100-km sides.

In terms of N_e, the average longwave surface flux F, over an area that is compared to individual clouds, is

$$F = (1 - N_e)F_{clear} + N_e F_{overcast} .$$

(1)

F_{clear} is the clear-sky flux; the flux that would occur if the broken cloud field was removed. $F_{overcast}$ is the flux that would occur if the broken cloud field became completely overcast. N_e is the fractional sky coverage of flat black plates. Here the longwave effective cloud fraction (N_e) is described and compared to measurements from the total sky imager (TSI), during the Cloudiness Intercomparison field campaign (February-May 2003, Southern Great Plains [SGP] Central Facility).

Instruments and Measurements

Re-arranging Eq. (1) to solve for N_e and substituting F_{pyr} for F yields:

$$N_e = \frac{F_{pyr} - F_{clear}}{F_{overcast} - F_{clear}} .$$

(2)

In Han and Ellingson (1999), longwave parameterizations were found for cumulus cloud fields. In that study, F_{pyr}, F_{clear}, and $F_{overcast}$ were obtained through measurements, fixing N_e. That process is used here for all skies.

Several datasets from the SGP Central Facility were used to derive N_e. The longwave (0-3000 cm^{-1}) downward flux, F_{pyr}, was measured directly by pyrgeometer. The radiances and surface emitting

temperature from the Atmospheric Emitted Radiance Interferometer (AERI), (Felz et al. 1998), and cloud base from Active Remote Sensing of Cloud Layers (ARSCL), (Clothiaux et al. 2000), were used to derive the F_{clear} and $F_{overcast}$ throughout the day. The resulting N_e are compared to the TSI opaque total sky cover, the fraction of the TSI hemispherical view taken up by opaque clouds.

This method, like others based on longwave surface measurements, (e.g., Durr and Philipona [2004]) has the advantage having continuous coverage, daytime and nighttime. The disadvantage is that clouds become difficult to detect when there is larger gaseous emission due to greater water vapor amounts and higher temperatures. The increased emission masks high/cold clouds. Active measurements at other wavelengths such as radar and lidar are able to "illuminate" high clouds. Passive shortwave methods such as Long and Ackerman (2000) are pseudo-active, using the sun for illumination.

Computing F_{clear} and $F_{overcast}$

The AERI takes calibrated radiance measurements of the downwelling radiance from 520 to 3020 cm^{-1} at approximately 0.5 cm^{-1} resolution. Adding the 5200 measured radiances, I_{AERI}, from 520 to 3020 cm^{-1} gives the total measured AERI radiance I_{AERI}^{tot}:

$$I_{AERI}^{tot} = \sum_{520cm^{-1}}^{3020cm^{-1}} I_{AERI} \qquad (3)$$

Assuming that the downwelling radiance outside the 833-1250 cm^{-1} window can be approximated by the Planck function (B_v), pseudo-window radiance (I_w) can be defined as:

$$I_w = I_{AERI}^{tot} - \int_{520\,cm^{-1}}^{833\,cm^{-1}} B_v(T_s, v)dv - \int_{1250\,cm^{-1}}^{3020\,cm^{-1}} B_v(T_s, v)dv \qquad (4)$$

A low standard deviation in the AERI 990cm^{-1} radiance combined with a high I_w indicates the presence of clouds. If an overcast threshold radiance is used, the observed I_w is considered an overcast radiance, $I_w^{overcast}$, when $I_w \geq I_{thold}$(overcast). A low standard deviation and low I_w indicates clear skies. When using a clear threshold, I_w is considered to be a clear radiance, I_w^{clear}, when $I_w \leq I_{thold}$(clear). The values of I_{thold}(overcast/clear) change according to the surface temperature and water vapor amounts.

The clear and overcast fluxes can be computed from I_w according to:

$$I_{AERI}^{tot,clear} = I_w^{clear} + \int_{520\,cm^{-1}}^{833\,cm^{-1}} B_v(T_s, v)dv + \int_{1250\,cm^{-1}}^{3020\,cm^{-1}} B_v(T_s, v)dv \qquad (6)$$

$$I_{AERI}^{tot,overcast} = I_w^{overcast} + \int_{520\,cm^{-1}}^{833\,cm^{-1}} B_\nu(T_s,\nu)d\nu + \int_{1250\,cm^{-1}}^{3020\,cm^{-1}} B_\nu(T_s,\nu)d\nu \qquad (7)$$

$$F_{clear} = LI_{AERI}^{tot,clear} + \pi \int_{0cm^{-1}}^{520cm^{-1}} B_\nu(T_{surf},\nu)d\nu + \delta_{pyr-AERI} \qquad (8)$$

$$F_{overcast} = LI_{AERI}^{tot,,overcast} + \pi \int_{0cm^{-1}}^{520cm^{-1}} B_\nu(T_{surf},\nu)d\nu + \delta_{pyr-AERI} \qquad (9)$$

L is a conversion factor ranging from π at the surface to 2.45 for clear skies. The integral of B_ν from 0-520 cm^{-1} is the flux from the opaque 0-520 cm^{-1} spectrum not measured by the AERI; δpyr-AERI is the instrument offset between the AERI and pyrgeometer. By iteration, clear and overcast radiances can be found and used to construct the clear and overcast fluxes. N_e is found using Eq. 2.

Comparing N_e to the Total Sky Imager

Two sets of threshold radiances were used to derive N_e. In the first, clear and overcast threshold radiances I_{thold}(clear) and I_{thold}(overcast) were specified based on monthly values. To increase sensitivity to clouds, the second used only the previous clear threshold I_{thold} (clear).

N_e for Clear and Overcast Threshold Radiances

Figure 1 shows ARSCL clear sky and lowest cloud base heights (Z_b) less than 4 km. Figure 1a shows the probability distribution function (pdf) of the TSI opaque total sky cover (shown in red) and the longwave N_e (shown in black). Figure 1a shows that the longwave N_e overestimates the number of clear-sky cases; this is probably due to the overcast threshold excluding actual cloud radiances.

Figure 1b is a binned scatter plot with the TSI opaque total sky cover on the x-axis and longwave N_e minus TSI opaque total sky cover on the y-axis, the bins are of width (along the x-axis) 0.1 between 0.05 to 0.95, and 0.05 starting at 0 and 0.95 respectively. The bins are of height 0.1 (along the y-axis) between -0.95 to 0.95, and 0.05 starting at -1 and 0.95. The horizontal line for N_e –TSI opaque=0 is shown in black. The black limiting lines showing N_e=1 (overcast) and N_e =0 (clear) run downwards from left to right. There can be no bins above the overcast limit line or below the clear limit. The result is 11 vertical stacks of bins; each stack corresponds to a range TSI opaque values. Each stack consists of 11 bins; each bin in the stack corresponds to a range of N_e – TSI opaque. The color of the bins in the stack indicates the percentage of the total number of cases in the stack contained in each bin. So if all the opaque TSI and N_e agree to within ±0.05 the scatter plot will be a single line of black bins at N_e – TSI opaque=0.

Figure 1b shows significant agreement at opaque TSI ≥0.95. So, the longwave N_e can identify overcast low clouds. The agreement at TSI ≤0.05 is somewhat spurious because from Figure 1a, the number of clear skies is greatly overestimated.
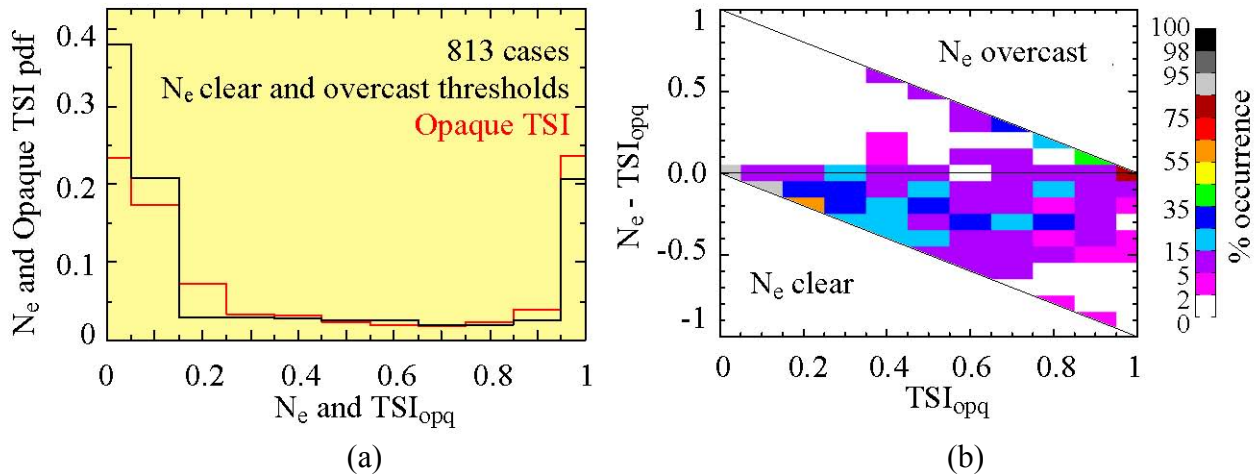
(a)   (b)

Figure 1. For ARSCL clear and clouds with Z_b < 4 km, clear and overcast thresholds. (a) N_e and opaque TSI probability distribution functions. (b) Binned longwave N_e – opaque TSI vs. opaque TSI.

Figure 2 compares the clear and overcast threshold N_e with TSI for medium clouds: 4 km $\leq Z_b$ < 8 km. From Figure 2a, the longwave N_e greatly overestimates the clear sky amount. Figure 2b shows that the N_e consistently underestimates the cloud amount. There is some agreement at opaque TSI ≥ 0.95, but much less than for Z_b<4km. This indicates that there are problems with longwave N_e as the clouds get higher.
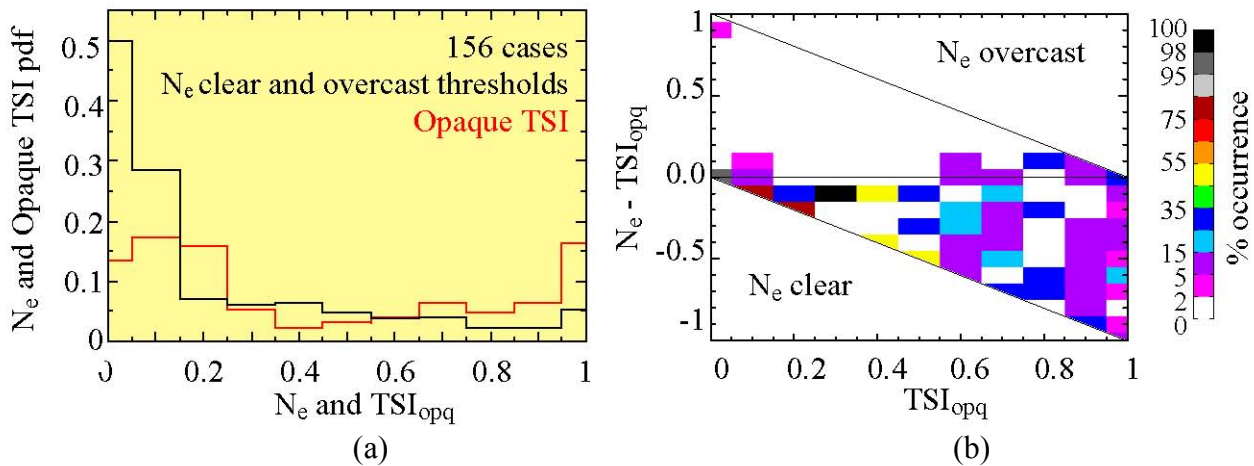

(a)   (b)

Figure 2. For ARSCL clear and clouds with 4 km $\leq Z_b$ < 8 km, clear and overcast thresholds. (a) N_e and opaque TSI probability distribution functions. (b) Binned longwave N_e – opaque TSI vs. opaque TSI.

Figure 3 shows the clear and overcast threshold N_e – TSI comparison for high clouds $Z_b \geq 8$ km. This illustrates the problem with detecting higher clouds using longwave instruments. From Figure 3a, the clear-sky amount is overestimated by a factor of 2. Figure 3b is a further indication of the insensitivity to high clouds, most of the high percentage bins are along the clear N_e line.
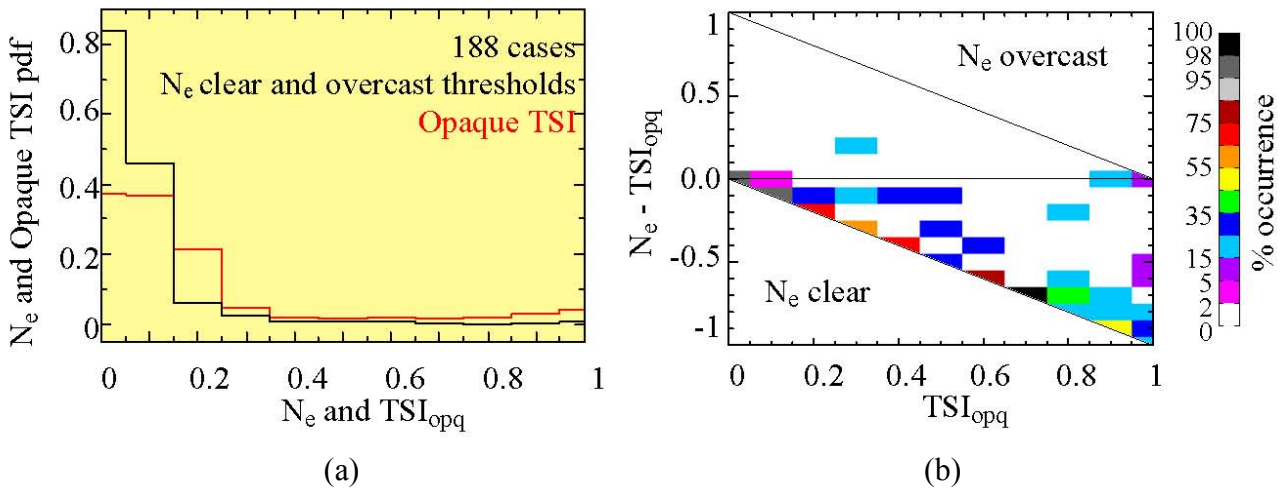
(a)   (b)

Figure 3. For ARSCL clear and clouds with $Z_b \geq 8$ km, Clear and overcast thresholds. (a) N_e and opaque TSI probability distribution functions. (b) Binned longwave N_e – opaque TSI vs. opaque TSI.

N_e for Clear Threshold Radiance

Figure 4 shows the threshold clear and overcast N_e – TSI comparison for clear sky and $Z_b < 4$ km with N_e derived using only the previous clear-sky threshold. This should be more sensitive to less emitting (colder or thinner) clouds; Figure 4a shows more agreement between the pdfs than Figure 1a. The increased sensitivity has the disadvantage of making large clear-sky radiances appear to be cloud radiances. This can be seen in Figure 4b, where a number of bins are along the N_e overcast limit line when the opaque TSI values are less than 0.8. As before, the binned plot shows significant agreement at opaque TSI$\geq$0.95.

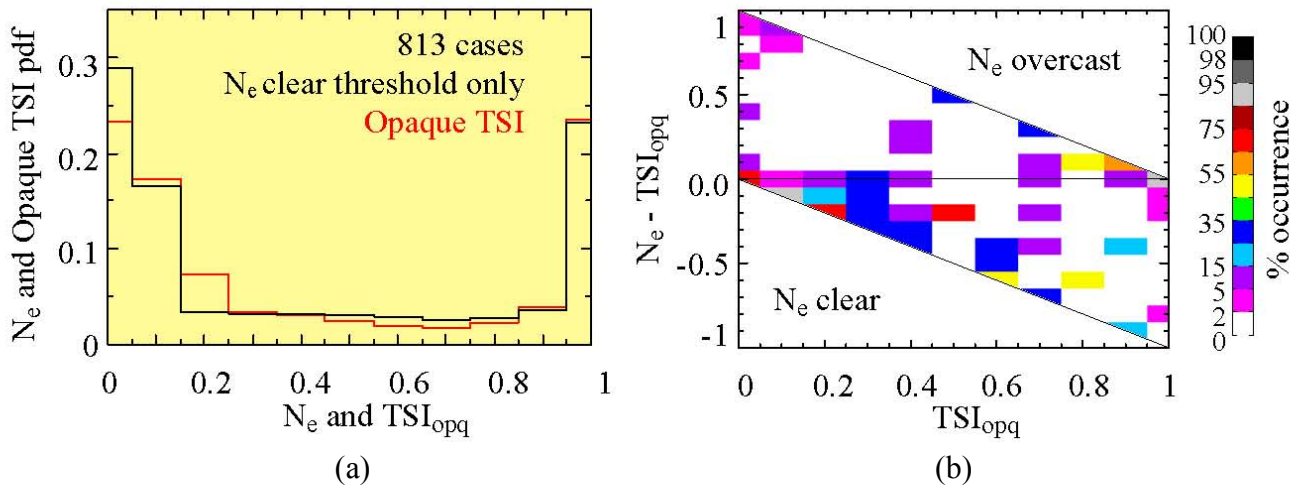(a)   (b)

Figure 4. For ARSCL clear and clouds with $Z_b < 4$ km, clear threshold. (a) N_e and opaque TSI probability distribution functions. (b) Binned longwave N_e – opaque TSI vs. opaque TSI.

Figure 5 shows the comparison for medium clouds: 4 km $\leq Z_b < 8$ km. Figure 5a shows that the attempt to increase cloud sensitivity still resulted in an overestimation of clear skies. The bins in Figure 5b are much more scattered than in Figure 2b; the similarity is the bins along the N_e overcast line, possibly due to problems with higher clouds. As with Figure 4b, the bins along the overcast line indicate too much sensitivity, leading to overestimates of cloud amount. The clear-sky overestimation can be seen in the bins along the N_e clear line.
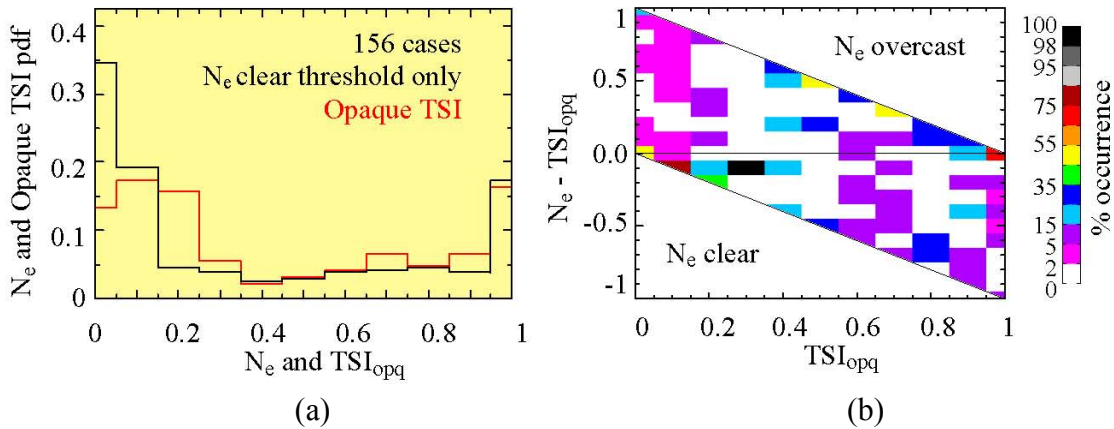

(a) (b)

Figure 5. For ARSCL clouds with 4 km $\leq Z_b < 8$ km, clear threshold. (a) N_e and opaque TSI probability distribution functions. (b) Binned longwave N_e – opaque TSI vs. opaque TSI.

Figure 6 shows the N_e - TSI comparison for high clouds; $Z_b \geq 8$km. Figure 6a shows that the N_e clear sky estimate is lower than Figure 3a, though it is still too high. Figure 6b shows some success in detecting higher clouds -- the section with TSI opaque>0.8 is more populated than in Figure 3b.

Using only a clear-sky threshold shows some improvement in detecting clouds with low emission, but the figures indicate that sensitivity to low-emitting clouds comes at the cost of overestimating the cloud amount. This may be addressed by more sophisticated thresholds for clear and overcast radiance.
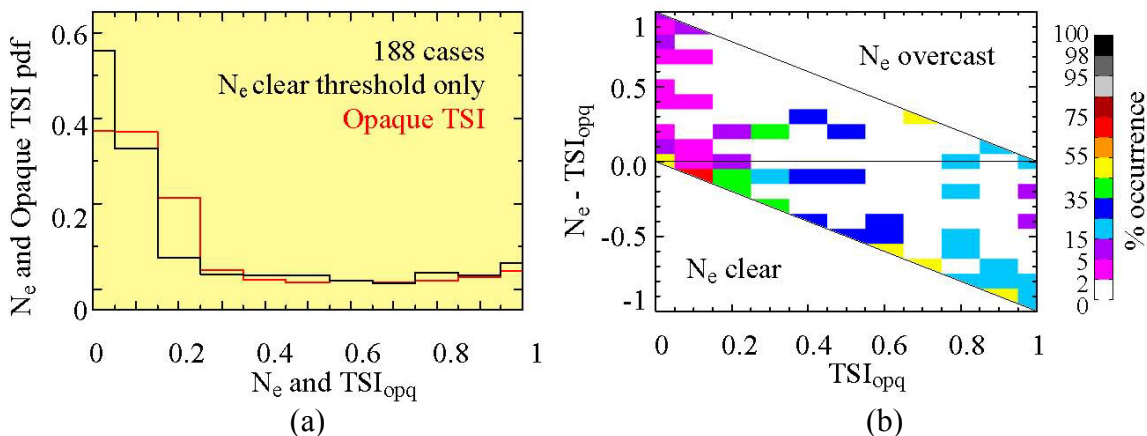

(a) (b)

Figure 6. For ARSCL clouds with $Z_b \geq 8$ km, clear threshold. (a) N_e and opaque TSI probability distribution functions. (b) Binned longwave N_e – opaque TSI vs. opaque TSI.

Summary and Conclusions

The results from two sets of thresholds for computing effective cloud fraction (N_e) were compared with the total sky cover for opaque clouds measured by the TSI. The first set used threshold values to determine clear sky and cloud radiances. The second used only the previous clear sky threshold. The N_e found using clear and cloud thresholds were almost always lower than the TSI opaque cloud amount. This N_e showed agreement with the TSI for clouds below 4 km. The agreement between N_e and TSI decreased for middle and high clouds. The N_e found using only the clear-sky threshold was more sensitive to low-emitting clouds, noticeable for the high clouds ($Z_b \geq 8$ km). The increase in sensitivity caused an overestimate of cloud amount, for middle (4 km $\leq Z_b < 8$ km) and low clouds ($Z_b < 4$ km).

Acknowledgments

References

Durr, B, and R Philipona. 2004. "Automatic cloud amount detection by surface longwave downward radiation measurements." *Journal of Geophysical Research* 109(D5)D05201.

Clothiaux, EE, TP Ackerman, GG Mace, KP Moran, RT Marchand, M Miller, and BE Martner. 2000. "Objective determination of cloud heights and radar reflectivities using a combination of active remote sensors at the ARM CART sites." *Journal of Applied Meteorology* 39, 645-665.

Felz, WF, WL Smith, RO Knuteson, HE Revercomb, HM Woolf, and HB Howell. 1998. "Meteorological applications of temperature and water vapor retrievals from the ground-based Atmospheric Emitted Radiance Interferometer (AERI)." *Journal of Applied Meteorology* 37, 857-875.

Han, D, and RG Ellingson. 1999. "Cumulus cloud parameterizations for longwave radiation calculations." *Journal of Atmospheric Science* 56, 837-851.

Long, CN, and TP Ackerman. 2000. "Identification of clear skies from broadband pyranometer measurements and calculation of downwelling shortwave cloud effects." *Journal of Geophysical Research* 105(D12)15609-15626.